The Novel Structure of a Pyridoxal 5′-Phosphate-Dependent Fold-Type I Racemase, α-Amino-ε-caprolactam Racemase from *Achromobacter obae*[†, ‡]

Seiji Okazaki,[§,||] Atsuo Suzuki,[§] Tsunehiro Mizushima,[§,⊥] Takeshi Kawano,[§] Hidenobu Komeda,[#] Yasuhisa Asano,[#] and Takashi Yamane*[,§]

Department of Biotechnology, Graduate School of Engineering, and Venture Business Laboratory, Nagoya University, Chikusa, Nagoya 464-8603, Japan, and Biotechnology Research Center, Toyama Prefectural University, Imizu, Toyama 939-0398, Japan

Received August 21, 2008; Revised Manuscript Received December 1, 2008

ABSTRACT: α-Amino-ε-caprolactam (ACL) racemase (ACLR) from *Achromobacter obae* catalyzes the interconversion of L- and D-ACL. ACLR belongs to the fold-type I group of pyridoxal 5′-phosphate (PLP) dependent enzymes. In this study, the first crystal structures of a fold-type I racemase are solved for the native form and ε-caprolactam-complexed form of ACLR at 2.21 and 2.40 Å resolution, respectively. Based on the location of ε-caprolactam in the complex structure, the substrate-binding site is assigned between Trp49 and Tyr137. The carboxyl group of Asp210 is a reasonable candidate that recognizes the nitrogen atom of a lactam or amide in the substrate. Based on a structural comparison with fold-type III alanine racemase, Tyr137 is potentially the acid/base catalytic residue that is essential for the two-base racemization mechanism. The overall structure of ACLR is similar to that of fold-type I enzymes. A structural comparison with these enzymes explains the different reaction specificities.

The soil bacteria *Achromobacter obae* produce an α-amino-ε-caprolactam (ACL)[1] racemase (ACLR, EC 5.1.1.15) in the cytoplasm (*1*). This racemase was isolated from *A. obae* in order to racemize D-aminolactam for industrial use (*2*). ACLR from *A. obae* is a pyridoxal 5′-phosphate (PLP) dependent enzyme that catalyzes the interconversion of L- and D-aminolactam, such as L- and D-ACL (*1, 2*) (Figure 1). ACLR is unique among racemases because it acts exclusively on a noncarboxylic compound, i.e., an intramolecular cyclic amide with an α-amino group (*1*).

This enzyme was used in combination with L-ACL hydrolase from *Cryptococcus laurentii* for industrial L-lysine production from D,L-ACL (*1, 3, 4*). Recently, amino acid amide racemizing activity was discovered in ACLR (*5*). Therefore, ACLR can be used in combination with a D-stereospecific amino acid amidase, such as D-aminopeptidase (DAP) (*6*), for D-amino acid production with 100% theoretical yield (*7, 8*).

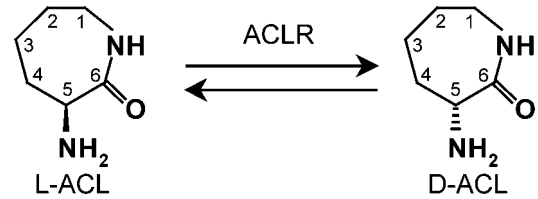

FIGURE 1: Reaction catalyzed by ACLR.

To date, all PLP-dependent enzymes whose structures have been solved are classified into at least five fold types, I−V, based on similarities in primary and secondary structures (*9*−*11*). There are no correlations between fold types and reaction types. The PLP-dependent racemases that have been identified to date are classified into fold types I, II, or III (*12*). ACLR is classified as a fold-type I group of PLP-dependent enzymes based on the amino acid sequence homology. The crystal structures of serine racemase, a fold-type II enzyme (PDB ID 1V71, 1WTC; unpublished), and alanine racemase, a fold-type III enzyme (*13*), were previously determined. However, the crystal structure of a racemase that belongs to fold-type I has not been determined.

The enzymes that belong to the fold-type I classification are well-characterized PLP-dependent enzymes (*11*). They invariably function as homodimers or higher order oligomers, with two active sites per dimer. They contain representative examples of multiple reaction types, such as decarboxylation and transamination. Therefore, comparing the structures of fold-type I enzymes with different reactions may indicate the reasons for these different mechanisms.

In this study, the crystal structure of native ACLR was determined at 2.21 Å resolution. The structures of ε-capro-

[†] This work was partly supported by a research grant (18380061) from the Japan Society for the Promotion of Sciences to Y.A.

[‡] Coordinate and structure factors of the native and ε-caprolactam complex structures have been deposited in the Protein Data Bank with accession codes 3DXV and 2ZUK.

* Corresponding author. E-mail: yamane@nubio.nagoya-u.ac.jp. Telephone: +8152 789 3339. Fax: +8152 789 3218.

[§] Department of Biotechnology, Graduate School of Engineering, Nagoya University.

[||] Venture Business Laboratory, Nagoya University.

[⊥] Present address: Department of Structural Biology and Biomolecular Engineering, Graduate School of Pharmaceutical Sciences, Nagoya City University, 3-1 Tanabe-dori, Mizuho-ku, Nagoya 467-8603, Japan.

[#] Biotechnology Research Center, Toyama Prefectural University.

[1] Abbreviations: ACL, α-amino-ε-caprolactam; ACLR, α-amino-ε-caprolactam racemase; PLP, pyridoxal 5′-phosphate; DAP, D-aminopeptidase; KPB, potassium phosphate buffer; GABA-AT, γ-aminobutyrate aminotransferase; AOA, aminooxyacetate; rms, root mean square; DGD, dialkylglycine decarboxylase; ε-cl, ε-caprolactam.

10.1021/bi801574p CCC: $40.75
Published on Web 01/15/2009

lactam and ACL are similar, and ε-caprolactam is reported to be a competitive inhibitor of ACLR (*1*). To determine the mechanism of both ε-caprolactam inhibition and substrate recognition, the crystal structure of ACLR complexed with ε-caprolactam was determined at 2.40 Å resolution. To our knowledge, this is the first structural report of a fold-type I racemase. The dimer is clearly the catalytically active entity. The candidate acid/base catalytic residue that is essential for the racemization reaction was assigned by comparing this structure to a fold-type III alanine racemase. In addition, comparisons with other fold-type I enzymes are also analyzed in order to understand different reaction specificities.

EXPERIMENTAL PROCEDURES

Protein Production, Crystallization, and X-ray Diffraction Data Collection. An *Escherichia coli* transformant expressing ACLR was prepared as follows. A modified DNA fragment encoding ACLR was obtained by PCR amplification using 50 μL of 10 mM Tris-HCl (pH 8.85), 25 mM KCl, 2 mM $MgSO_4$, 5 mM $(NH_4)_2SO_4$, 0.2 mM dNTP, sense and antisense primers (1 μM each), 2.5 units of *Pwo* DNA polymerase, and 500 ng of plasmid pACL60 (template) (*5*) for 2 min at 95 °C, followed by 30 cycles of 95 °C for 30 s, 55 °C for 30 s, and 72 °C for 2 min. The sense primer was 5′-GGCATAGCATATGACGAAGGCGCTTTACGATCG-3′ (*Nde*I recognition site underlined), and the antisense primer was 5′-ACTCCGTGGATCCACGTTTTACCAGCCAGCG-AACTGCGCGATTTC-3′ (*Bam*HI recognition site underlined). The amplified PCR product was digested with *Nde*I and *Bam*HI, separated by agarose gel electrophoresis, and then purified with a QIA quick gel extraction kit (Qiagen, Tokyo, Japan). The amplified DNA was inserted downstream of a T7 promoter in pET15b, yielding pET15ACL, which was used to transform *E. coli* BL21(DE3) cells.

E. coli BL21(DE3) harboring pET15ACL was subcultured at 37 °C for 12 h in a test tube containing 5 mL of LB medium supplemented with 80 μg/mL ampicillin. The subculture was then cultured at 37 °C for 5 h in 8 L of LB medium supplemented with 80 μg/mL ampicillin. Then 0.5 mM isopropyl β-D-thiogalactopyranoside was added to the culture, and the culture was incubated at 37 °C for an additional 5 h. The cells were harvested by centrifugation at 8000*g* for 10 min at 4 °C and washed with 0.85% NaCl. The buffer used throughout this study was 20 mM potassium phosphate buffer (KPB; pH = 7.0), containing 250 mM sucrose and 20 μM PLP. The cells were resuspended in 0.1 M buffer and disrupted by sonication for 10 min (19 kHz; Insonator model 201M; Kubota, Tokyo, Japan). To remove intact cells and cell debris, the lysate was centrifuged at 8000*g* for 10 min at 4 °C. The supernatant was heated at 60 °C for 10 min followed by centrifugation. The resulting soluble fraction was purified using Ni Sepharose high-performance (Amersham) and anion-exchange chromatography (HiTrapQFF). The His moiety was proteolytically removed with a thrombin protease, and the thrombin was removed by benzamidine Sepharose 6B.

ACLR crystals formed at 20 °C using the hanging-drop vapor diffusion method, with a mixture of 1.3 μL of protein (23.3 mg/mL) in buffer containing 70 mM KPB (pH = 7.0), 100 μM PLP, and 1.5 μL of reservoir solution [30% (w/v) PEG4000, 0.2 M magnesium chloride, 0.1 M Tris-HCl (pH 8.7), and 0.3 μL of additive solution (30% (w/v) sucrose)]. Hexagonal-shaped crystals grew to 0.05 mm × 0.05 mm × 0.03 mm in size within 14 days. The crystals belong to the space group $P2_1$, with a = 56.5 Å, b = 61.1 Å, c =105.2 Å, and β = 103.3°. There are two molecules per asymmetric unit. The crystals were directly frozen in a cold nitrogen stream at 100 K.

Table 1: Data Collection and Refinement Statistics

	native	ε-caprolactam complex
	Data Collection	
spacegroup	$P2_1$	$P2_1$
unit cell parameters		
a (Å)	56.5	56.6
b (Å)	61.1	60.7
c (Å)	105.2	105.3
β (deg)	103.3	103.1
wavelength (Å)	1.0	0.9
resolution (Å)[a]	50−2.21 (2.29−2.21)	50−2.40 (2.49−2.40)
R_{merge} (%)[a]	10.8 (49.4)	8.8 (35.9)
average $I/\sigma(I)$[a]	21.0 (2.8)	38.4 (7.0)
completeness (%)[a]	99.6 (98.2)	98.8 (98.6)
multiplicity[a]	5.9 (5.2)	4.8 (5.0)
	Refinement	
resolution (Å)	35.8−2.21	40.3−2.40
no. of unique reflections	33453	25532
R_{work}/R_{free}	0.197/0.245	0.191/0.251
no. of non-hydrogen atoms		
protein	6326	6287
ligand	30	46
water molecules	120	56
rms deviations		
bond lengths (Å)	0.009	0.010
bond angles (deg)	1.3	1.4
average B factor (Å^2)		
protein	31	42
PLP	22	33
ε-caprolactam		70
waters	26	32

[a] Values in parentheses are for the highest resolution shell.

ε-Caprolactam complex crystals were prepared by soaking native crystals in a solution of 30% (w/v) PEG4000, 0.2 M magnesium chloride, 0.1 M Tris-HCl (pH = 8.7), 2.9% (w/v) sucrose, 42 μM PLP, and 20 mM ε-caprolactam. As the soaking time increased, the diffraction quality of the crystal was severely deteriorated. As the diffraction quality of the native crystal was minimally deteriorated by soaking for 5 min in the soaking solution without 20 mM ε-caprolactam, we think that the deterioration of the soaked crystal supports binding of ε-caprolactam. Furthermore, the position and the *B*factor of ε-caprolactams in a 30 s soaked complex were almost the same as those for a 10 min soaked complex (data not shown). Therefore, 30 s was judged to be sufficient to form the ε-caprolactam complex. Diffraction data for native ACLR were collected at 100 K on beamline BL13B1 at NSRRC (Hsinchu, Taiwan). Diffraction data for the 30 s soaked ε-caprolactam complex was collected at 100 K on beamline BL44XU at SPring-8 (Hyogo, Japan). These data were processed and scaled using the HKL 2000 program package (*14*).

Structure Solution and Refinement. The data were subsequently processed using the CCP4 program suite (*15*). The native structure of ACLR was determined by molecular replacement using MOLREP (*16*) with a search model taken from γ-aminobutyrate aminotransferase (GABA-AT) of *E. coli* (PDB code 1SF2) (*17*), which has 29% amino acid sequence identity. Refinement and subsequent model building were performed using the programs REFMAC 5 (*18*) and COOT (*19*), respectively. Water molecules were added using

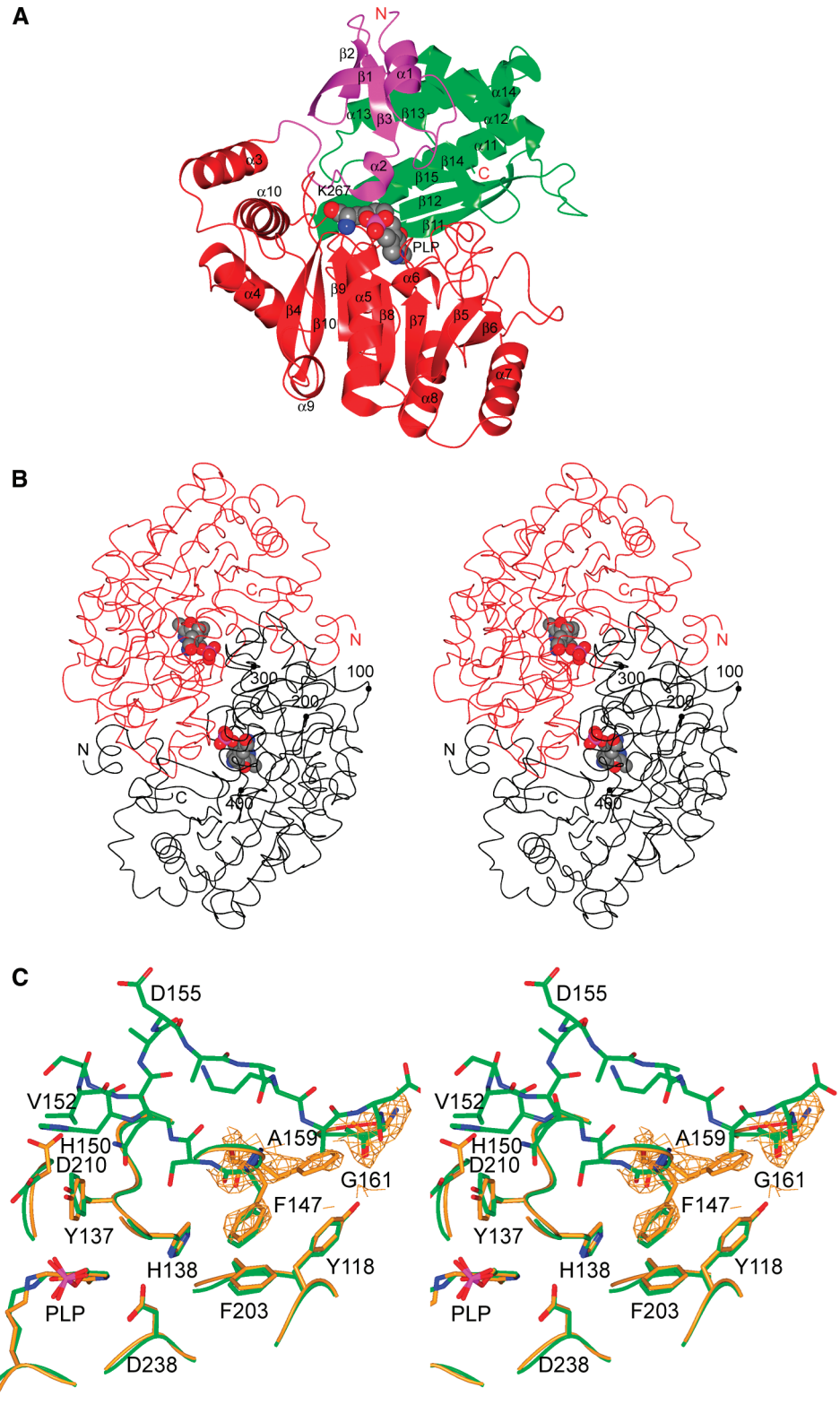

FIGURE 2: (A) Ribbon representation of a monomer of ACLR [prepared with CCP4MG (*35*)]. The amino and carboxy termini are denoted in red as N and C, respectively. Each of the three domains of ACLR is colored, the N-terminal domain (magenta), PLP-binding domain (red), and the C-terminal domain (green). PLP and Lys267 are represented as spheres; C atoms are in gray, O atoms in red, N atoms in blue, and P atoms in magenta. (B) Stereoview of the C^{α} trace and the two PLP cofactors of the ACLR dimer viewed along the molecular 2-fold symmetry axis. The two subunits are colored black and red, respectively. PLP and Lys267 are represented as spheres; C atoms are in gray, O atoms in red, N atoms in blue, and P atoms in magenta. The chain termini and every 100th C^{α} position of one subunit are labeled. (C) Stereo representation of the superposition of the active site of subunits A (orange) and B (green) of native ACLR. A σ_A-weighted $2F_o - F_c$ electron density map (1σ level; in orange) is superposed on residues Phe147 and G161 of subunit A. Residues 147−161 are represented as a ball and stick model.

the ARP/wARP 6.0 program (*20*). The initial phase set used for solving the ε-caprolactam complex was that of the native structure. Refinement and subsequent model building were performed the same as for native structure. The final model was validated with the program PROCHECK (*21*). Statistics for the final models are summarized in Table 1.

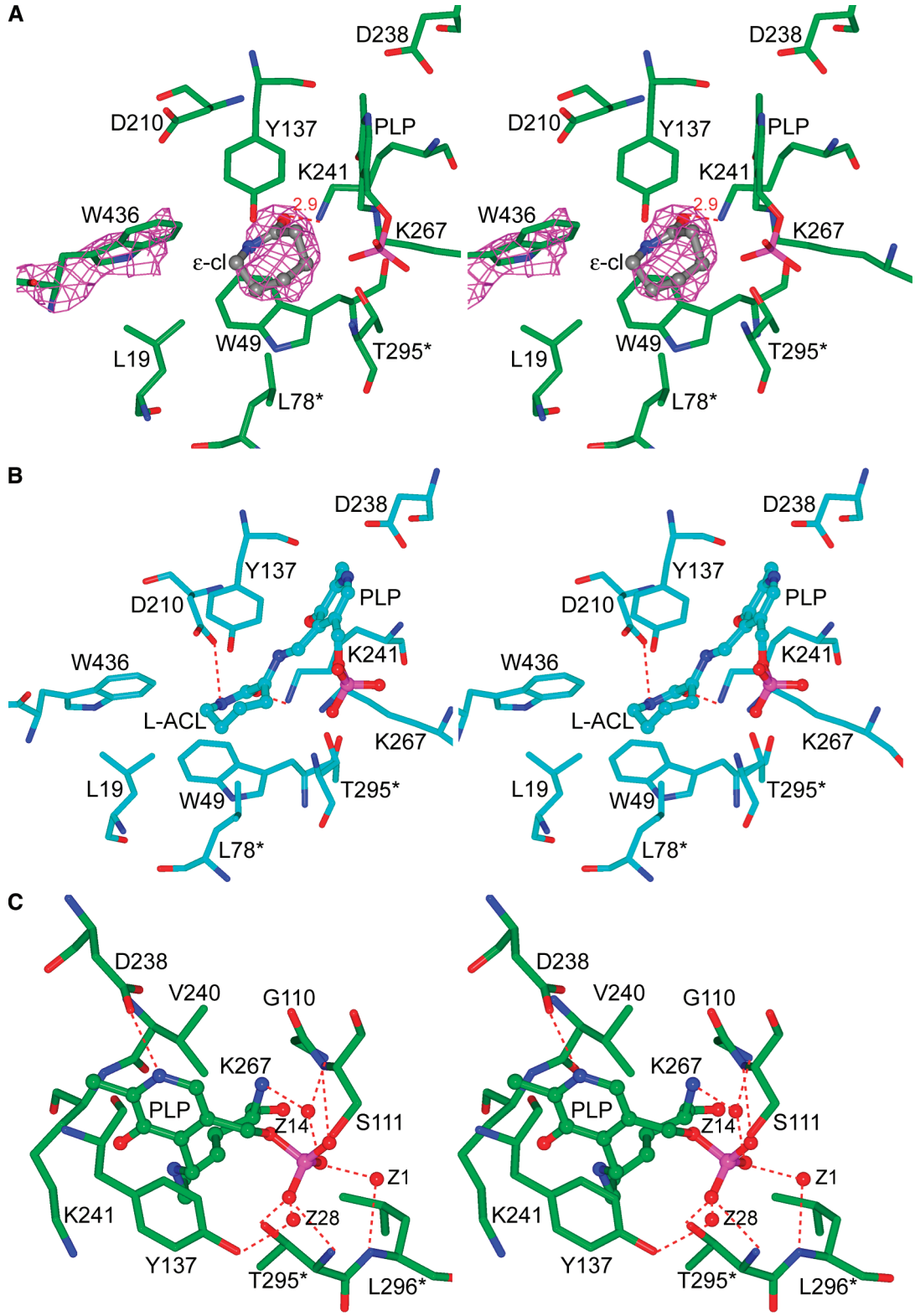

FIGURE 3: (A) Stereo representation of the active site of subunit B of ε-caprolactam (ε-cl) complexed with ACLR. ε-cl is represented as a ball and stick model, and ε-cl is shown in gray. Carbon atoms are shown in green. Residues contributed by subunit A are labeled with an asterisk (*). A σ_A-weighted $F_o - F_c$ omit map (Trp436 and ε-cl) contoured at 2.0σ calculated with data in the resolution range 10−2.4 Å is superposed in magenta. (B) Stereo representation of the energy-minimized model of the external aldimine (L-ACL-PLP) of L-ACL into the active site of subunit B of native ACLR. The external aldimine is represented as a ball and stick model. Carbon atoms are shown in cyan. Hydrogen bonds are shown as red broken lines. (C) Stereo representation of the active site of subunit B of native ACLR around PLP. PLP and Lys267 are represented as a ball and stick model. Residues contributed by subunit A are labeled with an asterisk (*). Hydrogen bonds are shown as red broken lines.

Model Building. The MOE (version 2006.08; Chemical Computing Group, Montreal, Canada) was used to construct the atomic model of the L-ACL-PLP external aldimine complex of ACLR and to perform energy minimization. First, the internal aldimine (PLP and Lys267) was deleted from subunit B of ACLR. Based on the *E. coli* GABA-AT

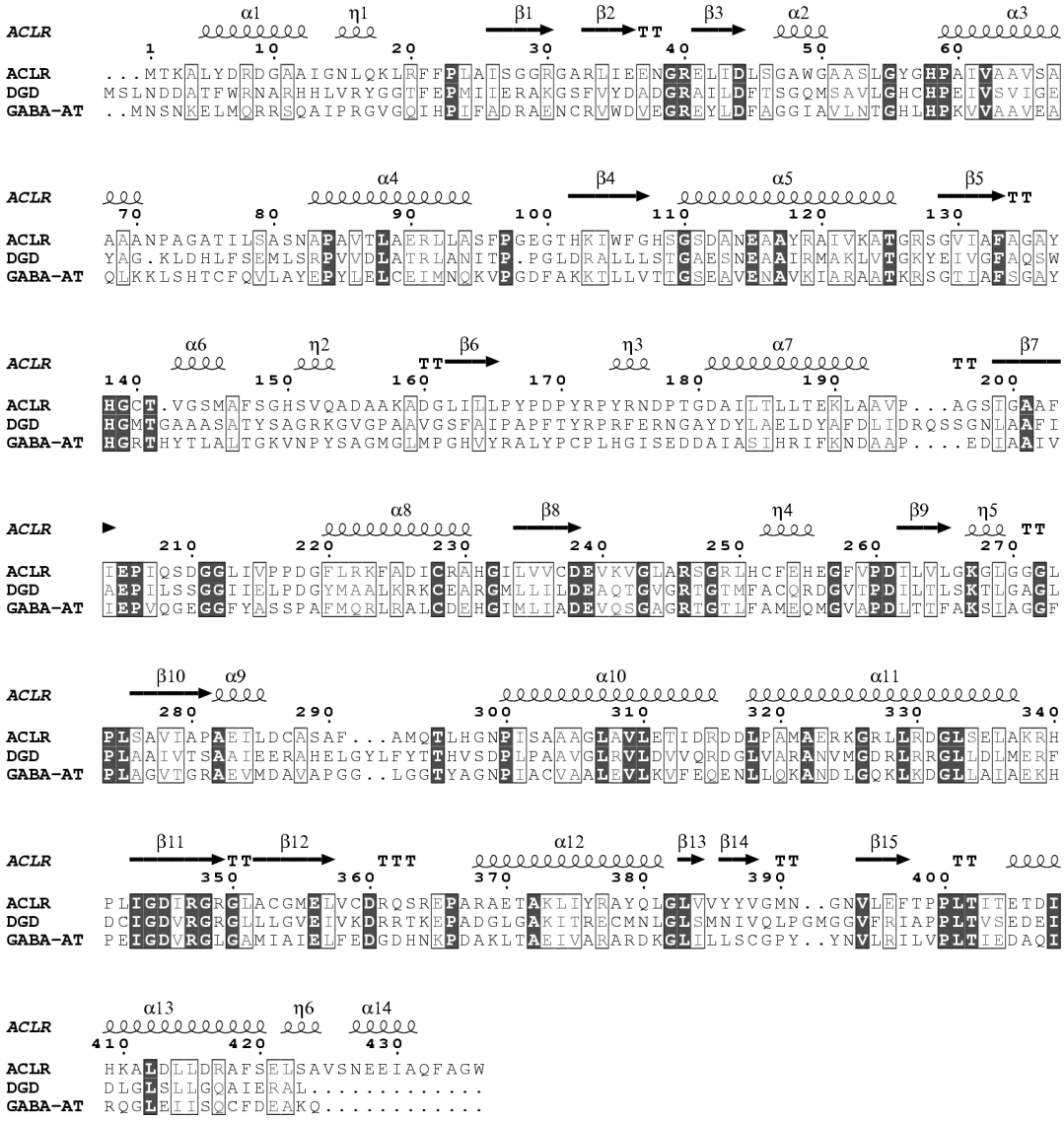

FIGURE 4: The alignment sequences of ACLR (ACLR), DGD (DGD), and *E. coli* GABA-AT (GABA-AT). The secondary structure elements are shown above the sequence. Conserved residues are boxed in white on a black background. Similar residues are boxed in black with a white background. This figure was produced using ClustalW.

complex with aminooxyacetate (AOA) (PDB code 1SFF), conformation of the Lys267 side chain of ACLR was changed. Then, the L-ACL-PLP model was introduced into the active site of subunit B of native ACLR by reference to the location and conformation of external aldimine AOA-PLP and ε-caprolactam in the complex. The atomic model of ACLR with the external aldimine was constructed by energy minimization with restraints on the protein atoms except hydrogen atoms.

RESULTS AND DISCUSSION

Overall Structure of the Monomer. The monomer structure can be subdivided into three domains: an N-terminal domain (residues 3−43), a C-terminal domain (residues 321−436), and a large PLP-binding domain (residues 48−319) (Figure 2A). The N-terminal domain contains two α-helices and a three-stranded antiparallel β-sheet. The PLP-binding domain comprises a central seven-stranded β-sheet surrounded by eight α-helices. The C-terminal domain is composed of four α-helices and a five-stranded β-sheet. The active site of the enzyme is centered around the PLP cofactor and is located in the cleft between the PLP-binding site and C-terminal domain of the protein.

Overall Structure of the Dimer. In the crystalline state, two subunit molecules in the asymmetric unit form a tightly packed homodimer (Figure 2B). Superposition of the two subunits gives the rms deviation = 0.38 Å for 420 (96%) structurally equivalent C^{α} atoms. The largest deviation is found in the loop region from residues 97 to 101, and the largest displacement (7.4 Å) was observed in the C^{α} of Glu99. Additionally, residues 149−160 were observed only in subunit B in the native structure, and the corresponding residues in subunit A were disordered (Figure 2C). Phe147 of subunit A appears to occupy two distinct positions. One of these positions is located at a hydrophobic pocket made by the Tyr118 and Phe203 side chains, similar to the position of Phe147 in subunit B. The other position is located near Tyr118 O^{η}. The position of the Phe147 side chain in subunit A near Tyr118 O^{η} is very close to the Ala159 side chain in subunit B (Figure 2C). Similarly, the position of the Asp210 side chain in subunit A is very close to the His150 side chain in subunit B. Approximately 4000 $Å^2$ of the solvent-

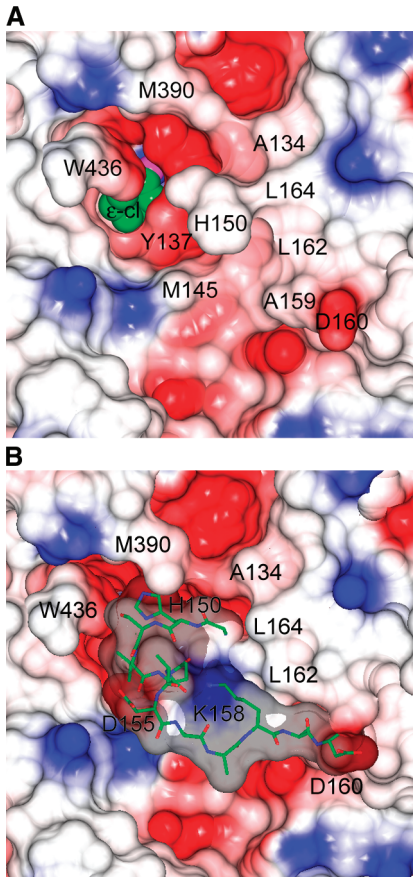

FIGURE 5: (A) Surface representation of the active site of subunit B in the ACLR−ε-cl complex. ε-cl is represented as a sphere model. (B) Surface representation of the active site of subunit B of native ACLR. Residues 149−160 are colored green and superimposed. The surface is colored according to the electrostatic potential of the residues (blue, positive; red, negative).

accessible surface area per monomer (approximately one-fourth of the monomer surface) is buried upon dimer formation. Subunits A and B in the dimer of native ACLR in the asymmetric unit are stabilized by 48 interchain hydrogen bonds (Supporting Information Table S1). In ACLR, the N-terminal domain of the subunit A interacts extensively with the PLP-binding domain of the subunit B like other fold-type I enzymes. This long list underscores the strength of the intersubunit interactions in this dimer and indicates that ACLR forms a dimer in solution like other fold-type I enzymes (*11*). The two PLP cofactors are located close to each other at the subunit interface of the dimer (the PLP phosphorus atoms are 16.2 Å apart).

ACLR and ε-Caprolactam Complex. The overall structure of ACLR complexed with ε-caprolactam is essentially the same as that of the native form except for the disordering of residues 151−158 in subunit B (Supporting Information Figure S1). The electron density of a σ_A-weighted $F_o - F_c$ omit map of the active site in the ε-caprolactam complex is shown in Figure 3A. A comparison of the omit map and the atomic *B* factors between ε-caprolactam and the neighboring Trp436 residue indicates that the occupancy of ε-caprolactam is comparable to that of Trp436 (Supporting Information Figures S2 and S3), and it is considered that ε-caprolactam is bound at the active site in this complex (Figure 3A). The ring of ε-caprolactam is sandwiched between the aromatic side chains of Trp49 and Tyr137. The carbonyl O of ε-caprolactam forms a hydrogen bond with Lys241 N^{ζ}. However, the residue that forms a hydrogen bond to the N of ε-caprolactam could not be assigned. From the omit map of ε-caprolactam, another binding mode generated by a 180° rotation around the C═O bond of ε-caprolactam in Figure 3A appears possible (Supporting Information Figure S4).

Because ε-caprolactam is reported to be a competitive inhibitor, the actual substrate, such as ACL, may be located at a position similar to where ε-caprolactam is located (Figure 3A). To predict the binding site and mode of the natural substrate and to identify the catalytically important residues, an energy-minimized model of the L-ACL-PLP external aldimine intermediate was produced by referring to the ε-caprolactam complex structure (Figure 3B). ACLR does not exhibit racemase activity toward D,L-amino acids but exhibits activity toward substrates containing the nitrogen of amides or lactams such as D,L-amino acid amides or D,L-cyclic amino lactams (*1, 5, 22*). Therefore, it is plausible to specify the residue that recognizes the nitrogen of amides or lactams. The structure of subunit B in native ACLR was chosen as a starting model because the position of Asp210 $O^{\delta 2}$ in this structure is suitable to form a hydrogen bond with the lactam N of L-ACL. In this model, the C5−H bond of L-ACL is oriented at the *si* face of PLP, and a hydrogen atom of the C5−H faces Lys267 N^{ζ} (the distance between C5 and Lys267 N^{ζ} is 3.1 Å). This observation agrees with the consideration described below that Lys267 is a candidate acid/base catalytic residue and indicates the plausibility of this model.

The Active Site. PLP is bound in a distinct cleft in the enzyme and is involved in many specific interactions (Figure 3C). The C4′ atom, which originally formed an aldehyde, connects covalently to the ε-amino group of Lys267 to form the internal aldimine (Schiff base) linkage (Supporting Information Figure S5). The pyridine nitrogen atom of PLP makes a salt bridge (about 2.8 Å) with Asp238 in ACLR. This interaction is the same as that of all known fold-type I enzymes (*11*). It is thought that Asp238 maintains the protonation of the nitrogen atom of PLP, thereby stabilizing the electron sink properties of PLP. This observation coincides with the expected basic racemization mechanism that proceeds through a quinonoid intermediate (*11*). The pyridine ring of PLP is sandwiched between Tyr137 and Val240. The phenolic hydroxyl group of Tyr137 interacts with the O2P in the PLP phosphate via water molecule Z28. Thr295* (from the neighboring subunit in the dimer) donates two hydrogen bonds from the main chain nitrogen and side chain oxygen atoms to the O2P of the phosphate group of PLP. The O1P of PLP forms two hydrogen bonds to Ser111 at the main chain nitrogen and side chain oxygen atoms. The O3P of PLP forms hydrogen bonds to two water molecules, Z1 and Z14.

The unique residues near the ACLR active site are Trp436 and Asp210. ACLR has 12 or 13 additional unique residues at its C-terminus compared to other fold-type I enzymes (Figure 4). The C-terminal residue Trp436 extends into the active site and forms part of the active site cavity. The indole ring of Trp436 is stabilized by Leu19 through a hydrophobic interaction. Although the role of Trp436 in ACLR function is unclear, based on its location, Trp436 may be important for substrate specificity. On the other hand, the carboxyl group of the Asp210 side chain points toward the active site

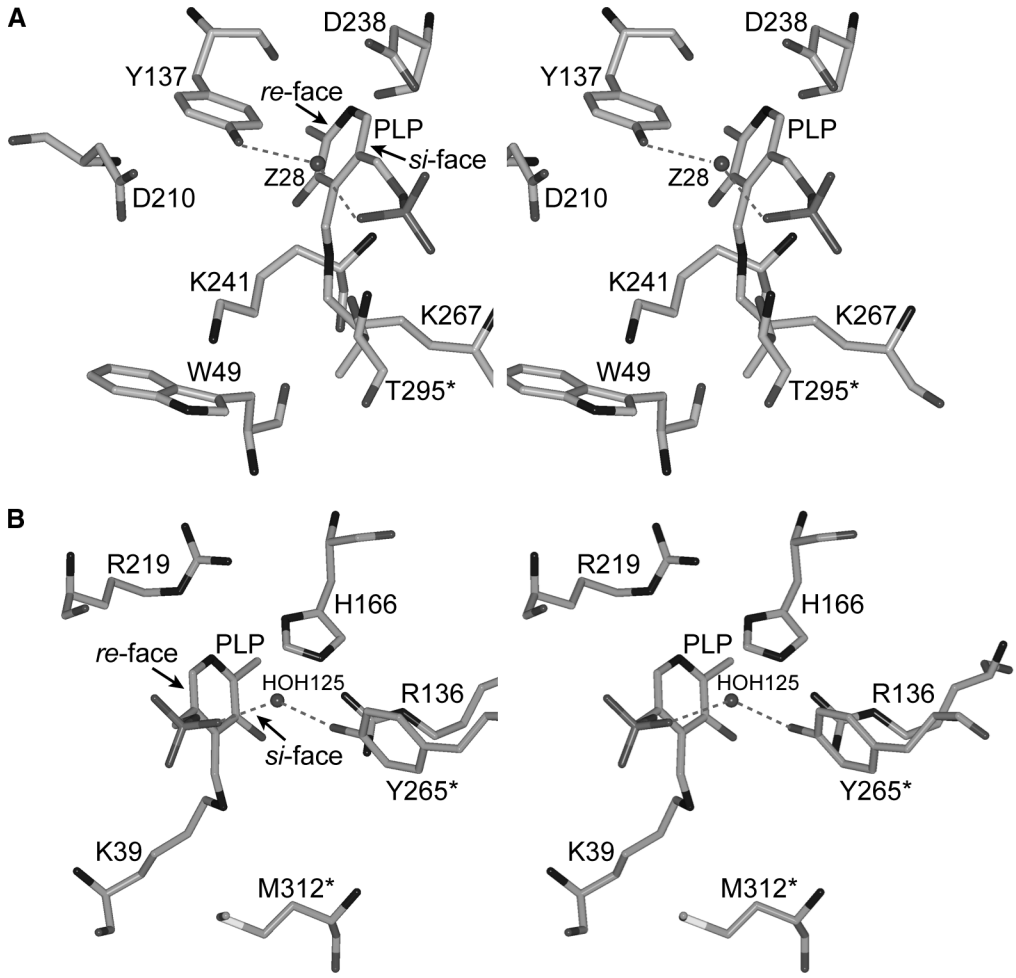

FIGURE 6: (A) Stereo representation of the active site residues of subunit B in native ACLR viewed from the *re* face of PLP. We suppose that the substrate enters from the *re* face of PLP to the active site. (B) Stereo representation of the active site residues of subunit B in native alanine racemase viewed from the *si* face of PLP. The alanine racemase substrate comes in from the *si* face of PLP.

only in subunit B of the native structure. This conformation of Asp210 is interesting because there is a possibility that the carboxyl group of Asp210 plays a role in recognizing the nitrogen of an amide or lactam in the substrate (Figure 3B).

Flexibility of Loop 149−160. Loop 149−160 is visible only in subunit B of native ACLR. This may be due to different crystal packing around the residues in the 149−160 loop, especially Asp155. The carboxyl group of Asp155 in subunit B of native ACLR forms bifurcated hydrogen bonds to Lys410 N^{ζ} in neighboring subunit A as an intermolecular contact, resulting in the loop order. In contrast, in subunit A of native ACLR the carboxyl group of Glu41 in neighboring subunit B replaces the basic Lys410 N^{ζ}. The loss of the intermolecular interaction between the loop and the neighboring subunit may lead to loop disorder in subunit A of native ACLR.

Because residues 151−158 are observed in subunit B of a native ACLR that was soaked for 5 min in a solution without ε-caprolactam, residues 151−158 in subunit B get disordered by soaking in solution containing ε-caprolactam (Figure 5A). One potential reason for this disordering is that the above-mentioned hydrogen bond between Asp155 in subunit B and Lys410 in neighboring subunit A was disrupted in soaked ε-caprolactam and resulted in disordering 151−158 loop. In fact, the electron density of the Lys410 side chain in neighboring subunit A in the ε-caprolactam complex is weaker than that in the native structure.

Loop 149−160 is considered to be flexible in solution because the substrate cannot access the active site if these residues remain ordered like those in subunit B of native ACLR (Figure 5B). The flexibility of the loop may come from Gly149 and Gly161, which work as a hinge in the loop. The flexibility of the loop also comes from weak interactions with the remaining region of ACLR. Only Ala159 N forms a hydrogen bond to Ala146 O, and hydrophobic interactions are observed only between the side chains of Val152 and that of Tyr137 and Trp436 in subunit B of native ACLR.

Comparison with Fold-Type III Alanine Racemase. Alanine racemase (EC 5.1.1.1) belongs to the fold-type III group and is an extensively investigated PLP-dependent racemase (*23*). It employs a two-base mechanism with Tyr265* and Lys39 (*11, 24−26*). The overall structure of ACLR is quite different from that of alanine racemase. However, the positions of Tyr137 O^{η} and the Asp210 side chain in ACLR, which are situated on the *re* face of the PLP ring, symmetrically correspond to that of Tyr265* O^{η} and the Arg136 side chain of alanine racemase, which are situated on the *si* face of the PLP ring, respectively (Figure 6A,B). Therefore, if racemization of ACLR proceeds via a two-base mechanism, Tyr137 as well as Lys267 may be candidate acid/base catalytic residues. However, there remains some possibility

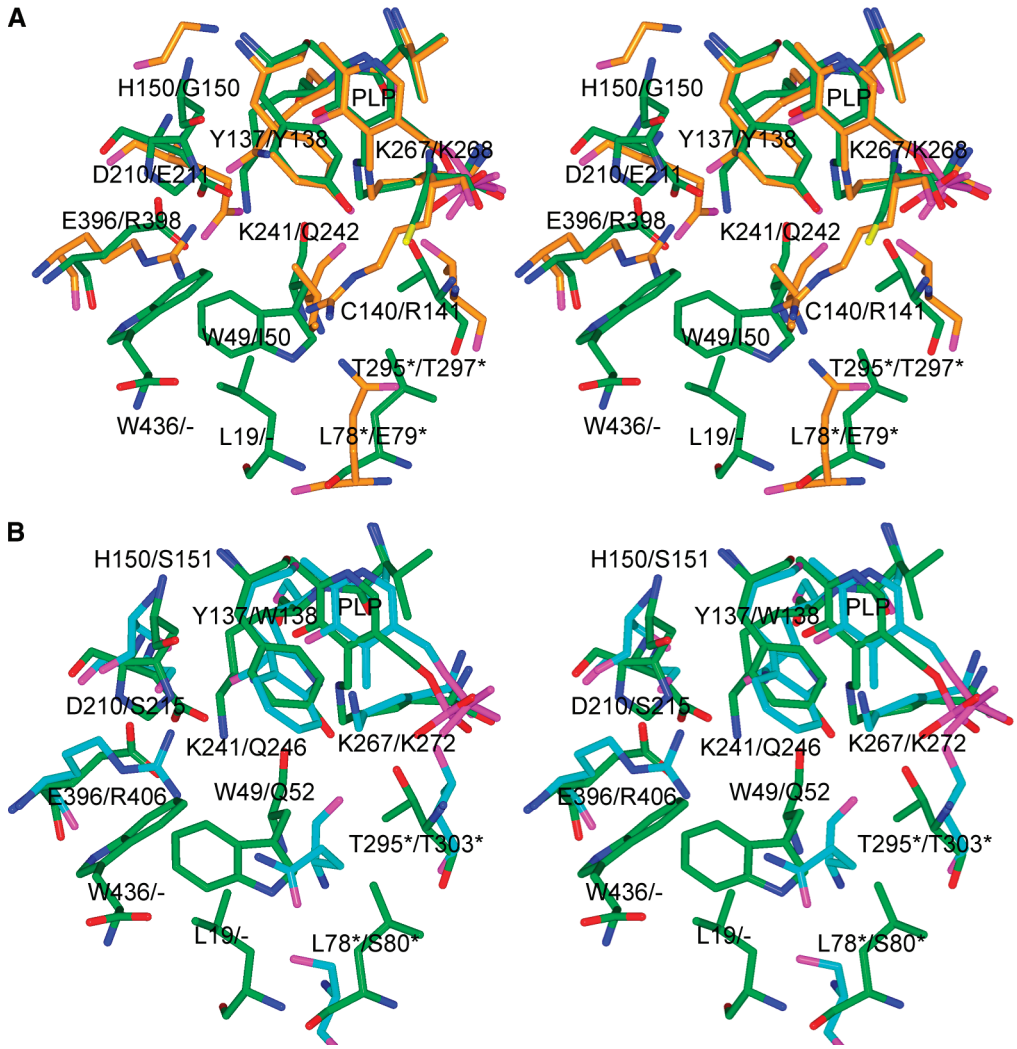

FIGURE 7: (A) Stereo representation of the superposition of the active sites of ACLR (green) and *E. coli* GABA-AT (orange). (B) Stereo representation of the superposition of the active sites of ACLR (green) and DGD (blue).

that Asp210 $O^{\delta 1}$ is an acid/base catalytic residue instead of Tyr137 (Figure 3B). In alanine racemase, the NH1 of Arg136 and the main chain nitrogen of Met312* form the recognition site for the carboxyl group of the substrate (*27*) and contribute to fixation of the substrate suited for progressing the racemization reaction. In ACLR, Asp210 may contribute to the recognition of the nitrogen of an amide or lactam in the substrate and may fix the substrate suited for progressing the racemization reaction.

The remarkable difference between alanine racemase and ACLR is the residue near the pyridine nitrogen of PLP. Asp238 in ACLR is located in the corresponding site of Arg219 in alanine racemase. As mentioned above, because the acidic residue Asp238 stabilizes the protonated pyridine nitrogen of PLP, the racemization mechanism of ACLR via the quinonoid intermediate is plausible. On the other hand, the racemization mechanism of alanine racemase, which is currently under discussion (*26, 28*), may be different from that of ACLR. In particular, Spies and Toney suggested that it proceeds via a quinonoid intermediate with a nonprotonated pyridine nitrogen of PLP (*28*). Because the protonation state of the pyridine nitrogen differs, the racemization mechanisms of ACLR and alanine racemase are probably not identical.

Comparison with Other Fold-Type I Enzymes. ACLR shows significant sequence identity with *E. coli* GABA-AT (*17*) (29% sequence identity with ACLR) and dialkylglycine decarboxylase (DGD) (*29*) (30% with ACLR) as shown in Figure 4. Supporting Information Figures S6A and S6B show overlays of the C^{α} traces of these enzymes. The location and conformation of the PLP of ACLR are consistent with those of *E. coli* GABA-AT and DGD. The overall fold of ACLR is similar to that of *E. coli* GABA-AT and DGD. In addition, *E. coli* GABA-AT and DGD also form dimers. A superposition of ACLR and *E. coli* GABA-AT results in C^{α} rms deviations of 1.53 Å at the monomer level and 1.97 Å at the dimer level for all structurally homologous C^{α} atoms. Similarly, a superposition of ACLR and DGD results in C^{α} rms deviations of 1.62 Å at the monomer level and 2.04 Å at the dimer level for all structurally homologous C^{α} atoms.

However, ACLR is unique among fold-type I enzymes in terms of additional C-terminal residues (Figures 4 and S6). Furthermore, the C-terminal residue Trp436 of ACLR extends into the active site and blocks the pathway that allows substrate access to the active site in subunit B of native ACLR (Figure 5B), as residues 15−17 in a closed form of a fold-type I aspartate aminotransferase (*30*). In *E. coli* GABA-AT and DGD, there is a pathway corresponding to positions Trp436 and Leu19 of ACLR, and this pathway is considered to play a role in allowing the substrate access to the active site.

Figure 7A presents an overlay of the active site residues of ACLR with *E. coli* GABA-AT. *E. coli* GABA-AT catalyzes transamination in its normal catalytic cycle. Generally, the transamination reaction requires one base, Lys, at the active site (*11*). Lys268 in *E. coli* GABA-AT works as the base and binds to PLP. Tyr137, which is considered to be the candidate acid/base catalytic residue of ACLR, is surprisingly conserved as Tyr138 in *E. coli* GABA-AT. However, Tyr138 in *E. coli* GABA-AT may not be necessary for GABA-AT activity because this residue is replaced by Phe189 in pig liver GABA-AT (*31*). Moreover, other fold-type I transaminases, such as human ornithine aminotransferase, have Phe177 located in this position (*32*).

The γ- and α-carboxylate groups of substrate α-ketoglutarate of *E. coli* GABA-AT are thought to be recognized by the guanidium groups of Arg141 and Arg398, respectively (*17*). In ACLR, these residues are replaced by Cys140 and Glu396, respectively.

Figure 7B presents an overlay of the active site residues of ACLR with DGD. DGD catalyzes both decarboxylation and transamination in its normal catalytic cycle. The decarboxylation-dependent transamination reaction proceeds by a one-base mechanism with Lys272, similar to the transamination reaction (*22*). Tyr137 of ACLR is replaced by Trp138 in DGD. Therefore, the presence or absence of an acid/base residue located at the opposite face of the cofactor viewed from the active site Lys may make a difference in reaction specificity.

The decarboxylation specificity of DGD is thought to be largely governed by the presence of Gln52 (*33*). This residue is replaced by Trp49 in ACLR. Additionally, Arg406 in DGD, which is thought to recognize the carboxylate of the substrate during transamination, is replaced by Glu396 in ACLR.

CONCLUSIONS

The crystal structures of native and ε-caprolactam complexed ACLR have been solved at 2.21 and 2.40 Å resolution, respectively. Based on the ACLR structure, the candidate acid/base catalytic residue, which is essential for the two-base racemization mechanism, is identified as Tyr137. Furthermore, the racemization mechanism of ACLR, as an example of a fold-type I racemase, is speculated to proceed via a quinonoid intermediate because of the presence of Asp238 near the pyridium nitrogen of PLP. This ACLR structural information will not only help structure/function studies on fold-type I racemases but also facilitate the molecular design of ACLR for industrial use. Additional mutational or kinetic studies are needed to confirm the role of Tyr137 as an acid/base catalytic residue, as was shown for alanine racemase (*24, 34*). Furthermore, similar to alanine racemase (*26*), structural analyses of the ACLR complex with reaction intermediate analogues are needed to understand the substrate recognition mechanism and to confirm the role of Asp210 as a recognition site for the nitrogen of an amide or lactam in the substrate.

ACKNOWLEDGMENT

The synchrotron radiation experiments were performed at SPring-8 with approval from the members of BL44XU (Proposal No. 2007A6940) and at NSRRC with approval from the members of BL13B1. We thank Dr. Eiki Yamashita of Osaka University for kind help with data collection at SPring-8. We thank Dr. Yuch-Cheng Jean of NSRRC and Prof. Nobuhisa Watanabe of Nagoya University for kind help with data collection at NSRRC. We are grateful to Prof. Tohru Yoshimura of Nagoya University for carefully reviewing the manuscript and providing helpful comments.

SUPPORTING INFORMATION AVAILABLE

Atomic distances within potential hydrogen bonds between the subunit of a native ACLR dimer, a figure showing the loop disordering by OMIT map, an OMIT map of Trp436 and ε-caprolactam, a figure indicating the atomic *B* factors of the ε-caprolactam complex, a figure showing alternative binding modes of ε-caprolactam, an OMIT map of the internal aldimine, and superpositions of ACLR on other fold-type I enzymes. This material is available free of charge via the Internet at http://pubs.acs.org.

REFERENCES

1. Ahmed, S. A., Esaki, N., Tanaka, H., and Soda, K. (1983) Properties of α-amino-ϵ-caprolactam racemase from*Achromobactor obae*. *Agric. Biol. Chem. 47*, 1887–1893.
2. Fukumura, T. (1977) Bacterial racemization of α-amino-ϵ-caprolactam. *Agric. Biol. Chem. 41*, 1321–1325.
3. Ahmed, S. A., Esaki, N., Tanaka, H., and Soda, K. (1986) Mechanism of α-amino-ϵ-caprolactam racemase reaction. *Biochemistry 25*, 385–388.
4. Fukumura, T. (1977) Conversion of D- and DL-alpha-amino-epsilon-caprolactam into L-lysine using both yeast cells and bacterial cells. *Agric. Biol. Chem. 41*, 1327–1330.
5. Asano, Y., and Yamaguchi, S. (2005) Discovery of amino acid amides as new substrates for α-amino-ϵ-caprolactam racemase from *Achromobacter obae*. *J. Mol. Catal. B: Enzym. 36*, 22–29.
6. Asano, Y., Nakazawa, A., Kato, Y., and Kondo, K. (1989) Properties of a novel D-stereospecific aminopeptidase from *Ochrobactrum anthropi*. *J. Biol. Chem. 264*, 14233–14239.
7. Asano, Y., and Yamaguchi, S. (2005) Dynamic kinetic resolution of amino acid amide catalyzed by D-aminopeptidase and α-amino-ϵ-caprolactam racemase. *J. Am. Chem. Soc. 127*, 7696–7697.
8. Yamaguchi, S., Komeda, H., and Asano, Y. (2007) New enzymatic method of chiral amino acid synthesis by dynamic kinetic resolution of amino acid amides: use of stereoselective amino acid amidases in the presence of α-amino-ϵ-caprolactam racemase. *Appl. Environ. Microbiol. 73*, 5370–5373.
9. Grishin, N. V., Phillips, M. A., and Goldsmith, E. J. (1995) Modeling of the spatial structure of eukaryotic ornithine decarboxylases. *Protein Sci. 4*, 1291–1304.
10. Soda, K., Yoshimura, T., and Esaki, N. (2001) Stereospecificity for the hydrogen transfer of pyridoxal enzyme reactions. *Chem. Rec. 1*, 373–384.
11. Eliot, A. C., and Kirsch, J. F. (2004) Pyridoxal phosphate enzymes: mechanistic, structural, and evolutionary considerations. *Annu. Rev. Biochem. 73*, 383–415.
12. Yoshimura, T., and Goto, M. (2008) D-Amino acids in the brain: structure and function of pyridoxal phosphate-dependent amino acid racemases. *FEBS J. 275*, 3527–3537.
13. Shaw, J. P., Petsko, G. A., and Ringe, D. (1997) Determination of the structure of alanine racemase from *Bacillus stearothermophilus* at 1.9-Å resolution. *Biochemistry 36*, 1329–1342.
14. Otwinowski, Z., and Minor, W. (1997) Processing of X-ray diffraction data collected in oscilation mode. *Methods Enzymol. 276*, 307–326.
15. Collaborative Computational Project, No. (1994) The CCP4 suite: programs for protein crystallography. *Acta Crystallogr., Sect. D: Biol. Crystallogr 50*, 760–763.
16. Vagin, A. A., and Isupov, M. N. (2001) Spherically averaged phased translation function and its application to the search for molecules and fragments in electron-density maps. *Acta Crystallogr., Sect. D: Biol. Crystallogr. 57*, 1451–1456.
17. Liu, W., Peterson, P. E., Carter, R. J., Zhou, X., Langston, J. A., Fisher, A. J., and Toney, M. D. (2004) Crystal structures of

unbound and aminooxyacetate-bound *Escherichia coli* gamma-aminobutyrate aminotransferase. *Biochemistry 43*, 10896–10905.
18. Murshudov, G. N., Vagin, A. A., and Dodson, E. J. (1997) Refinement of macromolecular structures by the maximum-likelihood method. *Acta Crystallogr., Sect. D: Biol. Crystallogr. 53*, 240–255.
19. Emsley, P., and Cowtan, K. (2004) Coot: model-building tools for molecular graphics. *Acta Crystallogr., Sect. D: Biol. Crystallogr. 60*, 2126–2132.
20. Perrakis, A., Morris, R., and Lamzin, V. S. (1999) Automated protein model building combined with iterative structure refinement. *Nat. Struct. Biol. 6*, 458–463.
21. Laskowski, R. A., MacArthur, M. W., Moss, D. S., and Thornton, J. M. (1993) PROCHECK: a program to check the stereochemical quality of protein structure. *J. Appl. Crystallogr. 26*, 283–291.
22. Ahmed, S. A., Esaki, N., Tanaka, H., and Soda, K. (1985) Mechanism of inactivation of α-amino-ϵ-caprolactam racemase by α-amino-δ-valerolactam. *Agric. Biol. Chem. 49*, 2991–2997.
23. Toney, M. D. (2005) Reaction specificity in pyridoxal phosphate enzymes. *Arch. Biochem. Biophys. 433*, 279–287.
24. Sun, S., and Toney, M. D. (1999) Evidence for a two-base mechanism involving tyrosine-265 from arginine-219 mutants of alanine racemase. *Biochemistry 38*, 4058–4065.
25. Watanabe, A., Kurokawa, Y., Yoshimura, T., and Esaki, N. (1999) Role of tyrosine 265 of alanine racemase from *Bacillus stearothermophilus*. *J. Biochem. 125*, 987–990.
26. Watanabe, A., Kurokawa, Y., Yoshimura, T., Kurihara, T., Soda, K., and Esaki, N. (1999) Role of lysine 39 of alanine racemase from *Bacillus stearothermophilus* that binds pyridoxal 5′-phosphate. Chemical rescue studies of Lys39 → Ala mutant. *J. Biol. Chem. 274*, 4189–4194.
27. Watanabe, A., Yoshimura, T., Mikami, B., Hayashi, H., Kagamiyama, H., and Esaki, N. (2002) Reaction mechanism of alanine racemase from *Bacillus stearothermophilus*. X-ray crystallographic studies of the enzyme bound with N-(5′-phosphopyridoxyl)alanine. *J. Biol. Chem. 277*, 19166–19172.
28. Spies, M. A., and Toney, M. D. (2007) Intrinsic primary and secondary hydrogen kinetic isotope effects for alanine racemase from global analysis of progress curves. *J. Am. Chem. Soc. 129*, 10678–10685.
29. Toney, M. D., Hohenester, E., Cowan, S. W., and Jansonius, J. N. (1993) Dialkylglycine decarboxylase structure: bifunctional active site and alkali metal sites. *Science 261*, 756–759.
30. McPhalen, C. A., Vincent, M. G., Picot, D., Jansonius, J. N., Lesk, A. M., and Chothia, C. (1992) Domain closure in mitochondrial aspartate aminotransferase. *J. Mol. Biol. 227*, 197–213.
31. Storici, P., De Biase, D., Bossa, F., Bruno, S., Mozzarelli, A., Peneff, C., Silverman, R. B., and Schirmer, T. (2004) Structures of γ-aminobutyric acid (GABA) aminotransferase, a pyridoxal 5′-phosphate, and [2Fe-2S] cluster-containing enzyme, complexed with γ-ethynyl-GABA and with the antiepilepsy drug vigabatrin. *J. Biol. Chem. 279*, 363–373.
32. Storici, P., Capitani, G., Muller, R., Schirmer, T., and Jansonius, J. N. (1999) Crystal structure of human ornithine aminotransferase complexed with the highly specific and potent inhibitor 5-fluoromethylornithine. *J. Mol. Biol. 285*, 297–309.
33. Fogle, E. J., Liu, W., Woon, S. T., Keller, J. W., and Toney, M. D. (2005) Role of Q52 in catalysis of decarboxylation and transamination in dialkylglycine decarboxylase. *Biochemistry 44*, 16392–16404.
34. Watanabe, A., Yoshimura, T., Mikami, B., and Esaki, N. (1999) Tyrosine 265 of alanine racemase serves as a base abstracting α-hydrogen from L-alanine: the counterpart residue to lysine 39 specific to D-alanine. *J. Biochem. 126*, 781–786.
35. Potterton, L., McNicholas, S., Krissinel, E., Gruber, J., Cowtan, K., Emsley, P., Murshudov, G. N., Cohen, S., Perrakis, A., and Noble, M. (2004) Developments in the CCP4 molecular-graphics project. *Acta Crystallogr., Sect. D: Biol. Crystallogr. 60*, 2288–2294.

BI801574P